

Annual Review of Materials Research

Hydrous Transition Metal Oxides for Electrochemical Energy and Environmental Applications

James B. Mitchell, Matthew Chagnot, and Veronica Augustyn

Department of Materials Science and Engineering, North Carolina State University, Raleigh, North Carolina, USA; email: jbmitch4@ncsu.edu, mschagno@ncsu.edu, vaugust@ncsu.edu

Annu. Rev. Mater. Res. 2023. 53:1-23

The *Annual Review of Materials Research* is online at matsci.annualreviews.org

https://doi.org/10.1146/annurev-matsci-080819-124955

Copyright © 2023 by the author(s). This work is licensed under a Creative Commons Attribution 4.0 International License, which permits unrestricted use, distribution, and reproduction in any medium, provided the original author and source are credited. See credit lines of images or other third-party material in this article for license information.

ANNUAL CONNECT

www.annualreviews.org

- Download figures
- Navigate cited references
- Keyword search
- Explore related articles
- Share via email or social media



Keywords

transition metal oxides, energy storage, energy conversion, insertion, electrochemistry, structural water

Abstract

Hydrous transition metal oxides (TMOs) are redox-active materials that confine structural water within their bulk, organized in 1D, 2D, or 3D networks. In an electrochemical cell, hydrous TMOs can interact with electrolyte species not only via their outer surface but also via their hydrous inner surface, which can transport electrolyte species to the interior of the material. Many TMOs operating in an aqueous electrochemical environment transform to hydrous TMOs, which then serve as the electrochemically active phase. This review summarizes the physicochemical properties of hydrous TMOs and recent mechanistic insights into their behavior in electrochemical reactions of interest for energy storage, conversion, and environmental applications. Particular focus is placed on first-principles calculations and operando characterization to obtain an atomistic view of their electrochemical mechanisms. Hydrous TMOs represent an important class of energy and environmental materials in aqueous and nonaqueous environments. Further understanding of their interaction with electrolyte species is likely to yield advancements in electrochemical reactivity and kinetics for energy and environmental applications.

1

1. INTRODUCTION

Hydrous transition metal oxides (TMOs) are materials that confine water within their bulk, either coordinated to a transition metal or present via secondary bonding within a cavity such as an interlayer. Many TMOs form hydrous analogs with structures that can be amorphous or crystalline, though a smaller number of TMOs exhibit the former. These materials are the outcome of synthesis performed in aqueous conditions, giving rise to lower densities and other unique physicochemical properties and electrochemical behavior as compared with their anhydrous counterparts. Hydrous TMOs are the focus of this review. As conceptualized by Ardizzone et al. (1), hydrous TMOs contain both an outer and an inner surface; the inner surface can be considered to be an extension of the outer electrochemical interface within the volume of the material (2). This is unlike in dense oxides, which interact with the electrolyte via only their outer surface. The possibilities of an increased electrochemical interface via the inner surface and the use of hydrous channels to transport protons, ions, and solvent molecules into the interior of a TMO serve as primary drivers for scientific and technological interest in hydrous TMOs (Figure 1). This review discusses the current understanding of the electrochemistry of hydrous TMOs as electrodes for electrochemical energy and environmental applications.

Hydrous TMOs contain structural water (confined within the bulk; see **Figure 1**), different from the surface-adsorbed water present at ambient conditions of all oxides. The structural water molecules are integral to the structural stability of the hydrous TMO. Many hydrous TMOs also contain charge-compensating ions in coordination with the structural water, as in the alkali ions that are present in the interlayer of birnessite (A_x MnO₂·nH₂O), a layered hydrous manganese oxide. This review first discusses the synthesis and physicochemical properties of hydrous TMOs. Then, it presents their electrochemical behavior, including the electrochemical insertion of protons and cations for energy storage, their electrocatalytic activity in aqueous electrolytes, and finally their use as electrodes for environmental applications, such as ion separation. We highlight

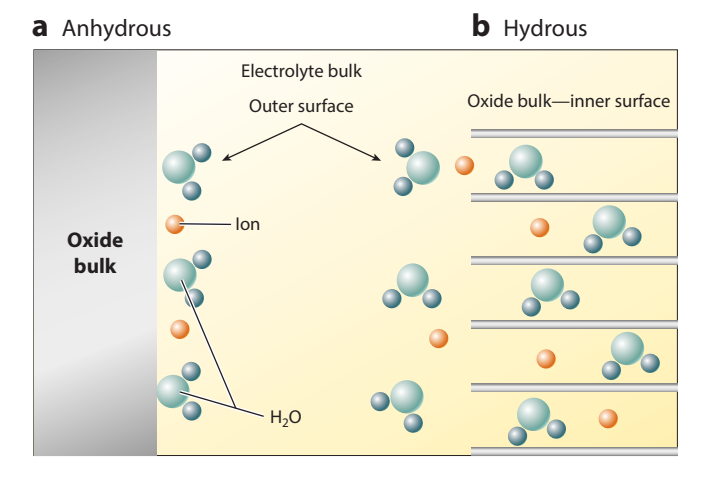


Figure 1

Comparison of the electrochemical interface of an (a) anhydrous versus (b) hydrous transition metal oxide (TMO). Both materials exhibit an outer surface that interacts with the electrolyte. Unlike anhydrous TMOs, the electrochemical interface of a hydrous TMO (b) can extend within its volume, giving rise to a large interfacial area—an inner surface—with the possibility for mass transport of electrolyte species into the bulk. Compared with anhydrous TMOs, hydrous TMOs exhibit low densities that may minimize structural distortions during electrochemical reactions, leading to fast kinetics and long lifetimes.

recent studies that provide a mechanistic understanding of the correlation between hydrous TMO properties and their electrochemical behavior.

2. MATERIALS CHEMISTRY OF HYDROUS TRANSITION METAL OXIDES

2.1. Synthesis of Hydrous Transition Metal Oxides

Most TMOs will form hydrous phases at low temperature and in the presence of water. Common synthesis routes include precipitation (3), sol-gel (4), electrochemistry (including electrodeposition and electrophoresis) (5), and ion-exchange reactions (6). Here, we provide examples of different synthesis routes for hydrous TMOs of interest for electrochemical energy and environmental applications. Hydrous TMOs obtained via precipitation reactions include crystalline hydrates of WO₃ and MoO₃ as well as hydroxides of Co and Ni (7). Freedman (3) described the synthesis of WO₃·2H₂O and WO₃·H₂O via their precipitation from tungsten salts such as Na₂WO₄ in strong acids. The resulting materials are crystalline nanoscale precipitates with platelet-like morphology. Electrochemistry in an aqueous electrolyte, such as anodization of a metal electrode (2), electrophoretic deposition of colloidal particles (8), and electrodeposition (9), can also yield hydrous TMOs. These techniques are useful for obtaining thin films of hydrous TMOs for fundamental electrochemical studies of their behavior with no additional components (e.g., conductive additives) that can confound analysis. Ion exchange in aqueous solutions or via electrochemical insertion reactions can also lead to the formation of hydrous TMOs including metastable phases. A prominent class is composed of materials containing ions, aligned in tunnels or layers, that can be exchanged with protons. For example, acid etching of Bi₂W₂O₉ leads to the formation of H₂W₂O₇ (or W₂O₆·H₂O) (10), the structure of which resembles that of WO₃·H₂O except that the water layers are separated by two tungsten oxide layers (11). Protonation and hydration can also occur during electrochemical cycling in an acidic electrolyte, as in the transformation of Li₃IrO₄ to H_{3,4}IrO₄ (12). Soaking Li₂RuO₃ in water for 30 days leads to the formation of a hydrous phase, Li_{0.75}H_{1.25}RuO₃, with the proposed mechanism involving the exchange of Li₂O with H₂O (13). During proton insertion, Li_{0.75}H_{1.25}RuO₃ exhibits order-of-magnitude-higher specific currents than Li₂RuO₃; the improvement is ascribed to the accessibility of bulk Ru redox upon hydration, which is, in effect, the activation of the inner surface.

Another mechanism of structural water uptake can occur during electrochemical cycling in a neutral pH electrolyte of layered alkali TMOs. Oxidation and concomitant removal of the alkali ions lead to increased electrostatic repulsion between the TMO layers, which favors the insertion of water molecules (14). For example, electrochemical oxidation of $Na_{0.67}Mn_{0.67}M_{0.33}O_2$ yields a hydrated layered phase, $Na_xMn_{0.67}M_{0.33}O_2 \cdot nH_2O$, where M is a third-row transition metal (15). The resulting materials have hydrated interlayers as well as an expanded, accordion-like morphology due to the large interlayer expansion. These synthesis routes demonstrate the many mechanisms by which hydrous TMOs form in ambient conditions, including indirect routes in aqueous electrolytes as illustrated by the hydration of Li_3IrO_4 and $Na_{0.67}Mn_{0.67}M_{0.33}O_2$. The hydrous TMOs discussed in this review are summarized in **Table 1**.

2.2. Structural Water Bonding in Transition Metal Oxides

Hydrous TMOs provide various bonding environments for structural water, including direct coordination to a transition metal as well as secondary bonding within a cavity. The local binding environment of water in TMOs dictates its physicochemical properties, such as thermal and chemical stability. A useful material to illustrate the coordination chemistry of structural water in TMOs is WO₃·2H₂O, which contains water molecules with two different bonding environments.

Table 1 Hydrous transition metal oxides of interest for electrochemical energy and environmental applications discussed in this review

Hydrous transition		Dimensionality of
metal oxide	Synthesis method	water networks
t-MnO ₂	Hydrothermal	1D
Birnessite (δ-MnO ₂)	Electrochemical	2D
$Na_xMn_{0.67}M_{0.33}O_2 \cdot nH_2O$	Solid state, electrochemical	2D
Hydrous V ₂ O ₅	Ion exchange, water exchange	2D
Hydrous Co(OH) ₂	Electrochemical	2D
Hydrous WO ₃	Acid precipitation, ion exchange	2D
Hydrous MoO ₃	Acid precipitation	2D
Hydrous iridates	Electrochemical	2D
Li _{0.75} H _{1.25} RuO ₃	Electrochemical, water exchange	2D
Hydrous RuO ₂	Sol-gel	3D

The structure of WO₃·2H₂O consists of corner-sharing WO₅(OH₂) octahedra with coordinated water molecules at the apices (**Figure 2a**) (16). These octahedra form a 2D network in the x-z crystallographic plane. The second type of structural water molecule is within the interlayer, forming a hydrogen-bound network of structural water (Figure 2b). The presence of water in the octahedral coordination of W leads to a shortening of the terminal W-O bond, which leads to the W=O stretching mode at \sim 948 cm⁻¹ in Raman or infrared spectroscopy (Figure 2c) (16). Dehydration of WO₃·2H₂O proceeds via two structural transformations: the loss of the secondary-bound water in the interlayer leads to the formation of orthorhombic WO₃·H₂O at ~100°C, while the loss of the water of coordination leads to WO₃ at 350°C. These differences in thermal stability are reflected in thermogravimetric analysis (Figure 2d). Secondary-bound structural water is the most prevalent in hydrous TMOs, where it is often accompanied by stabilizing cations. For example, in layered and tunneled manganese oxides, the presence of structural water and cations leads to a decrease in the average manganese oxidation state from 4+ (anhydrous) to between 3.5 and 3.9. A thermodynamic study of several manganese oxides, including birnessite, found that surface energy tends to decrease with decreasing average manganese oxidation state, where hydrous manganese oxides exhibit lower surface energies than the anhydrous oxides (17). The low surface energy of hydrous manganese oxides favors the formation of nanoscale particles, demonstrating how the local water and cation content of hydrous TMOs can impact their morphology and particle size.

The stability of structural water in hydrous TMOs depends on its bonding environment. Secondary-bound structural water can vaporize at relatively low temperatures (<100°C) while waters of coordination can be very stable (removed at >300°C). This means that the structural water content of TMOs can be affected by conditions during material preparation and characterization, such as (a) characterization of hydrous TMOs at low pressure [e.g., X-ray photoelectron spectroscopy (XPS), transmission electron microscopy (TEM)], (b) electrode slurry preparation in nonaqueous solvents like N-methyl-2-pyrrolidone (NMP), and (c) electrochemistry in aqueous and nonaqueous solvents. For example, in our research with hydrous WO₃, we found that TEM characterization must be performed under cryogenic conditions to preserve the interlayer water of WO₃·2H₂O (20). We also found that NMP and nonaqueous electrolyte solvents such as propylene carbonate can lead to dehydration of WO₃·2H₂O and a structural transition to WO₃·H₂O (21). WO₃·H₂O can form WO₃·2H₂O during cycling in an aqueous acidic electrolyte (22). Effects beyond dehydration are also possible, such as reactivity with solution species. For

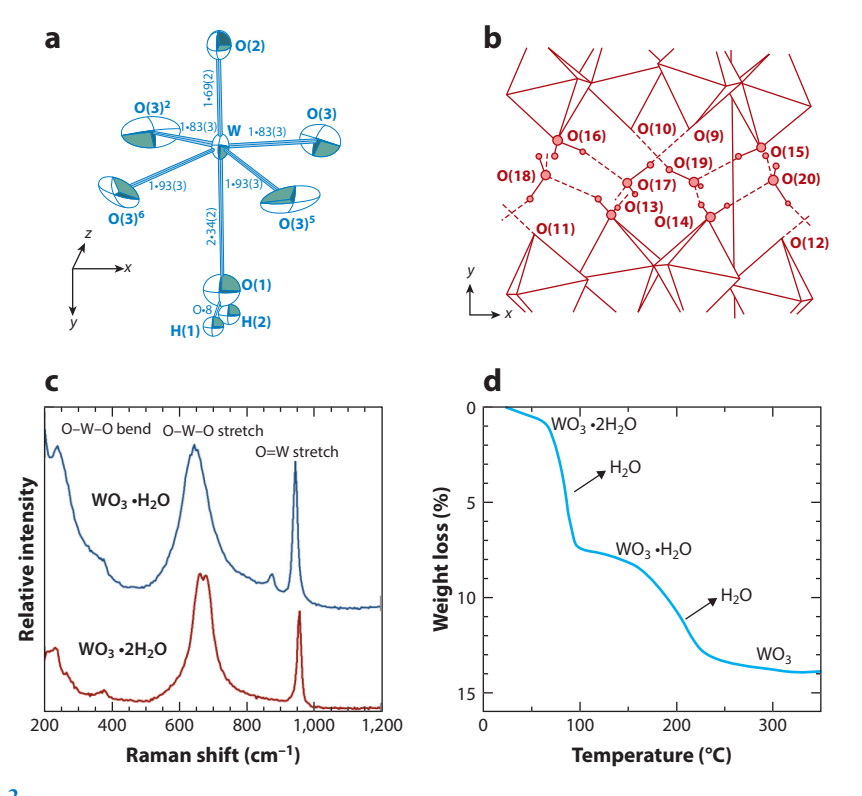


Figure 2

Structural chemistry of a crystalline hydrate, $WO_3 \cdot 2H_2O$. (a) Coordination of tungsten in $WO_3 \cdot 2H_2O$. Oxygen from the water of coordination, O(1), is directly bound to W, leading to a lengthening of that W–O bond. In turn, bonding of W with the terminal oxygen, O(2), is shorter, leading to a W=O stretching mode in spectroscopy measurements. Panel reproduced with permission from Reference 18. (b) Hydrogen bond network within the interlayer of $WO_3 \cdot 2H_2O$, formed by terminal oxygens, coordinated structural waters, and secondary-bound structural waters. Panel reproduced with permission from Reference 19. (c) Raman spectra of $WO_3 \cdot 2H_2O$ and $WO_3 \cdot H_2O$ powders. The presence of the interlayer structural water in $WO_3 \cdot 2H_2O$ shifts the W=O stretching (\sim 950 cm $^{-1}$) and O–W–O bending (600–800 cm $^{-1}$) modes as compared with $WO_3 \cdot H_2O$. Panel adapted with permission from Reference 16. (d) Thermogravimetric analysis of $WO_3 \cdot 2H_2O$ in air. The first major weight loss is dehydration to $WO_3 \cdot H_2O$, and the second weight loss step is due to dehydration to anhydrous WO_3 .

example, electrochemical cycling of a V₂O₅ aerogel in a nonaqueous Li⁺ electrolyte led to the formation of LiOH (23), which is proposed to occur because of the reactivity of Li⁺ with structural water in the aerogel. The reactivity of structural water molecules, driven by their pK_a, can also be utilized to synthesize inorganic/organic hybrid materials such as layered, alkylamine-intercalated tungsten oxides (24). To summarize, the stability of the structural water in TMOs can be affected by ambient pressure, temperature, humidity, and pH. TMOs containing structural water may undergo significant structural transformations, even phase transitions, upon dehydration. It is important to consider the hydration state at each step of materials preparation (e.g., physical characterization, electrode preparation, electrochemistry) to accurately correlate the composition and structure of a hydrous TMO with its properties. Operando and in situ characterization methods are very useful to determine the stability of materials containing structural water under experimental conditions.

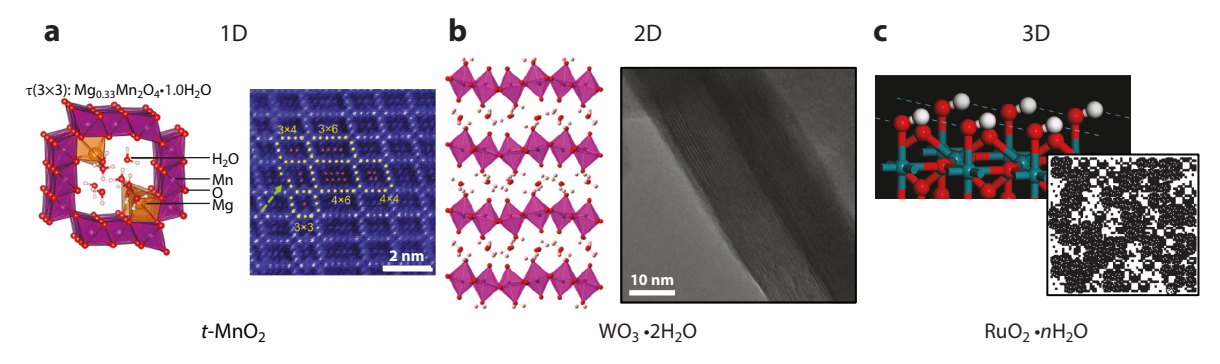


Figure 3

Dimensionality of structural water networks in hydrous TMOs. (a) Structure of t-MnO₂. Tunnels are formed from a 3 × 3 network of edge-sharing MnO₆ octahedra containing cations and structural water molecules, as shown on the left. Significant heterogeneity is possible, as shown in the atomic high-angle annular dark-field image on the right. Panel a (left) adapted with permission from Reference 36; copyright 2018 American Chemical Society. Panel a (right) adapted with permission from Reference 37. (b, left) Structure of WO₃·2H₂O with layers of corner-sharing WO₅(OH₂) octahedra separated by interlayer secondary-bound water. (b, right) A low-temperature, high-resolution transmission electron microscopy image of a platelet showing the hydrated interlayer. Panel adapted with permission from Reference 20; copyright 2017 American Chemical Society. (c, bottom) Schematic of RuO₂·nH₂O depicting rutile RuO₂ nanocrystals separated by hydrous grain boundaries that form a 3D structural water network throughout the volume of the material. (c, top) Neutron scattering and density-functional theory results indicate that the surface consists of Ru–OH with small amounts of hydrogen-bound water. Panel c (top) adapted with permission from Reference 31, copyright 2002 American Chemical Society.

2.3. Dimensionality of the Structural Water Network in Hydrous Transition Metal Oxides

Structural water molecules can form 1D, 2D, or 3D networks within TMOs (Figure 3). 1D structural water networks arise in hydrous TMOs with tunnels. A prominent example is manganese oxide, which can form tunnel structures of different sizes based on the number of edge-sharing MnO₆ octahedra. This includes hollandite (2 \times 2) and todorokite (3 \times 3); the numbers in parentheses indicate the number of octahedra along the length and width of the tunnel, respectively. Structural water in these materials is present along with alkali cations for charge balance. 2D water networks are found in layered hydrous TMOs. These include the tungsten oxide hydrates described previously and the molybdenum oxide hydrates that are isostructural with the tungsten oxide hydrates. The structural waters in the interlayer form 2D networks that separate the oxide layers (Figure 3b). Another prominent example is $V_2O_5 \cdot nH_2O$, which contains 2D water layers across the x-y plane (25), with waters randomly oriented within the 2D liquid network (26). The layered structure can take up more than a monolayer of interlayer structural water with increasing humidity (27). The stepwise changes in the hydration of the interlayer, as observed with X-ray diffraction (XRD), resulted in abrupt changes to the interlayer spacing as a function of temperature and relative humidity (28, 29). The intermolecular forces between the structural water and the oxide lattice can cause long-range structural changes to the solid-state structure. X-ray and neutron scattering, along with refinement of the pair distribution function, showed that the presence of interlayer structural water led to rearrangement of the V-O bilayers (30). 3D structural water networks can be found in amorphous and nanocrystalline hydrous TMOs. Examples include the hydrous grain boundaries in nanostructured RuO₂·nH₂O (Figure 3c) (31). The nanocrystalline surfaces are terminated with hydroxyl groups, leading to strong hydrogen bonding between near-surface disordered structural water molecules (32). Understanding the

dimensionality of the structural water network in TMOs is important because it defines the available transport pathways for electrolyte species.

2.4. Structural Water Dynamics in Hydrous Transition Metal Oxides

Structural water molecules in hydrous TMOs exist under confinement, which means that their arrangement and dynamics are determined by the geometry and chemistry of the TMO. It is important to understand structural water dynamics in hydrous TMOs because this can determine the kinetics of electrochemical processes involving their inner surfaces, such as mass transport of electrolyte species to and from the inner surface sites. In general, there are two extremes of structural water dynamics in hydrous TMOs: water molecules whose dynamics are severely restricted due to strong interaction with the TMO lattice and water molecules that behave more like bulk liquid water due to weak interactions with the TMO lattice. The former type of water dynamics would lead to limited mobility whereas the latter exhibits both translational and rotational motion. An illustrative comparison is between two hydrous TMOs with 2D structural water networks but different structural water dynamics: WO₃·2H₂O and V₂O₅·1.5H₂O. Due to the large neutron scattering cross section of hydrogen, neutron techniques are important for understanding the structure and dynamics of water in hydrous TMOs, particularly quasielastic neutron scattering (QENS) (33). Our work using QENS and solid-state ¹H nuclear magnetic resonance studies of the interlayer water in WO₃·2H₂O revealed no translational motion on the nanosecond to microsecond timescale (Figure 4a,b) (34). On the other hand, QENS of V₂O₅·1.5H₂O showed that

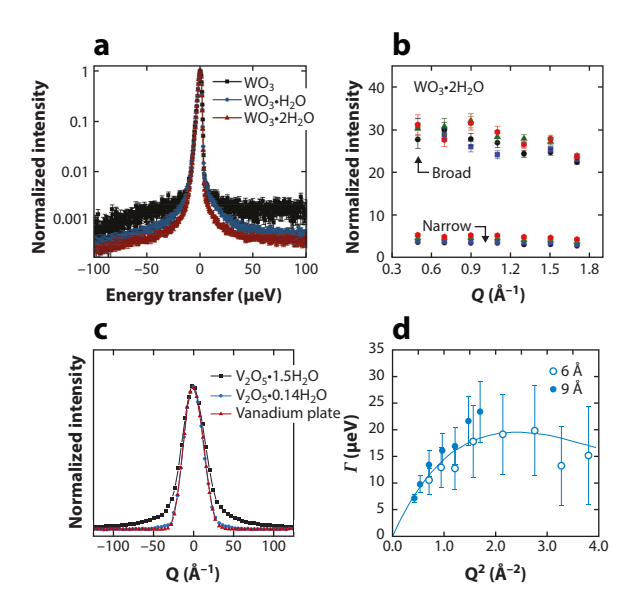


Figure 4

Dynamics of structural water in hydrous TMOs studied by quasielastic neutron scattering (QENS). (a) QENS of WO₃·2H₂O, WO₃·H₂O, and WO₃ at T=300 K and Q=0.7 Å⁻¹. (b) Peak fitting of the QENS region in WO₃·2H₂O showing a lack of Q-space dependence and thus no translational motion of structural water. (c) QENS of V₂O₅·1.5H₂O (black squares), V₂O₅·0.14H₂O (blue circles), and a vanadium plate (red triangles). (d) Q-dependence of the QENS half width at half maximum (HWHM), Γ , for V₂O₅·1.5H₂O showing translational motion of structural water with a diffusion coefficient of 3.3 × 10⁻¹⁰ m²/s. Panel b adapted with permission from Reference 34; copyright 2019 American Chemical Society. Panels c and d adapted with permission from Reference 26; copyright 2000 American Chemical Society.

the intermolecular forces between the host lattice and structural water lead to lower rotational and translational motion than bulk water but faster motion than ice, with the hypothesis that the interlayer water behaves as a 2D liquid (**Figure 4**c,d) (26). Water dynamics in hydrous TMOs are affected by other species in the interlayer, such as cations, which provides a further mechanism to tune structural water properties. For example, chemical intercalation of Zn²⁺ into a hydrous layered titanate increased the proton conductivity by three orders of magnitude (35). The interlayer Zn²⁺ ions are proposed to increase the self-dissociation of H₂O molecules and enhance proton transport via a Grotthuss-type mechanism.

Water confined in TMOs is also of interest for understanding nuclear quantum effects in condensed matter. Toward this goal, Lalik et al. (38) investigated structural water in $WO_3 \cdot H_2O$ with neutron diffraction, XRD, inelastic neutron scattering, and neutron Compton scattering. They proposed a new structural model for $WO_3 \cdot H_2O$ with better agreement with inelastic neutron scattering data and hypothesized that confinement of the structural water molecules in $WO_3 \cdot H_2O$ leads to nuclear quantum delocalization of protons. Future work must be performed to determine if nuclear quantum tunneling of protons is possible in $WO_3 \cdot H_2O$. The implications of these nuclear quantum effects in $WO_3 \cdot H_2O$ on its electrochemical behavior are not yet clear but provide an exciting avenue for future investigation. As a further motivation, theory has shown that nuclear quantum effects of water can affect such properties as the redox potential at the electrochemical interface, which may be of particular interest for electrocatalysis with hydrous TMOs (39).

3. HYDROUS TRANSITION METAL OXIDES FOR ELECTROCHEMICAL ENERGY STORAGE

Electrochemical insertion of cations and protons from liquid electrolytes into solid-state hosts is the dominant mechanism for electrochemical energy storage, particularly alkali-ion batteries (40). Ion insertion with fast kinetics is desirable to enable high-power devices. This process can be separated into fundamental steps, each associated with a time constant: (a) ion migration in the bulk electrolyte, (b) ion desolvation at the electrochemical interface, (c) charge transfer at the electrochemical interface, and (d) diffusion of the ion into the active material, away from the electrochemical interface. Depending on the electrochemical system, other steps may also be present, such as ion transport through a solid-electrolyte interphase, electrolyte transport through a porous electrode, and the nucleation of a new phase in the active material. Selection of the active material impacts the kinetics of ion desolvation, charge transfer, solid-state diffusion, and structural transformation. There are several hypotheses for what may make hydrous TMOs exhibit fast ion insertion kinetics: (a) a decrease of the energy barrier associated with ion desolvation at the electrochemical interface by providing a solvation environment within the material or an expanded interlayer that accommodates solvent molecules; (b) liquid-like ion transport within the solid state, such as via a Grotthuss-like mechanism for protons; and (c) a decrease of structural changes associated with ion insertion due to lower density, allowing solid-solution insertion or more facile structural transformations. Hydrous TMOs can undergo dynamic changes in composition and structure in an electrochemical environment, including structural water uptake, expulsion, and rearrangement upon electrochemical proton or cation insertion (Figure 5).

Hydrous TMOs are hypothesized to allow facile transport of electrochemically inserted protons along the structural water networks, rendering them attractive for proton-based energy storage devices (42–44). Protons can be electrochemically inserted into hydrous TMOs with different structural water network topologies: 1D [hexagonal WO₃ (h-WO₃)], 2D (WO₃·2H₂O), and 3D (RuO₂·nH₂O). h-WO₃ is a metastable hydrated form of WO₃ in which corner-sharing WO₆ octahedra form hexagonal tunnels filled with structural water aligned in 1D channels along the *z*-axis (**Figure 6***a*). Jiang et al. (45) investigated the proton insertion mechanism of h-WO₃

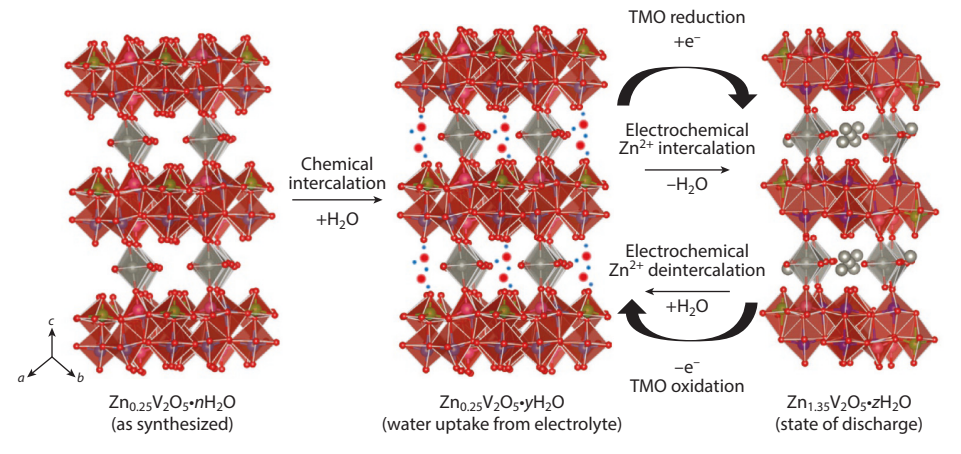


Figure 5

Dynamic evolution of a hydrous transition metal oxide (TMO) during electrochemical cation insertion. Hydrous TMOs can undergo changes in composition and structure in an electrochemical environment due to the possibility of ion exchange and chemical and electrochemical reactions between the material and electrolyte salt and solvent. This is illustrated by a hydrous vanadium oxide, which undergoes chemical intercalation of structural water from the electrolyte (without change of oxidation state), electrochemical intercalation of cations (with change of oxidation state), and structural water rearrangement and expulsion. Figure adapted with permission from Reference 41.

nanofibrils using electrochemical quartz crystal microbalance (EQCM) and ex situ XRD. Cyclic voltammetry showed two reversible proton insertion and deinsertion peaks with good reversibility and kinetics and with surface-controlled insertion between 1 and 10 mV/s. The material also had excellent cycling stability. The proposed proton insertion mechanism involved three distinct steps, including the expulsion of structural water molecules. This dynamic change in the structural water content may alleviate the distortion associated with proton insertion and increase kinetics. Sun et al. (46) utilized first-principles molecular dynamics (MD) to understand proton transport along the confined water molecules in h-WO₃ containing 0.08 H⁺. They found that the diffusivity of inserted protons along the 1D structural water channel exhibits a maximum when the structural water content per WO₃ is 0.5 (**Figure 6a,b**), attributed to an optimal linear density of water molecules in the tunnel to enable Grotthuss transport.

Our group investigated electrochemical proton insertion into the layered tungsten oxide hydrates, $WO_3 \cdot nH_2O$ (n=1,2). The structure and physical properties of these materials were discussed in Section 2. A general finding is that $WO_3 \cdot nH_2O$ exhibits faster proton insertion kinetics than WO_3 (20, 22, 34, 47), suggesting that the presence of structural water can promote proton transport. The electrochemical response of $WO_3 \cdot nH_2O$ appears more capacitive: Current-voltage responses are more symmetrical than those of WO_3 , indicative of a charge-storage process requiring less structural reorganization of the host (48). Utilizing operando XRD, we found that both WO_3 and $WO_3 \cdot 2H_2O$ undergo a reversible phase transition during proton (de)insertion (for $\sim 0.1 \text{ H}^+/\text{W}$; **Figure** $6c_*d$). However, the transformation occurs more rapidly in $WO_3 \cdot 2H_2O$. In fact, at fast timescales (<10 s), WO_3 does not transform and remains frozen in its original structure with a concomitant decrease in proton storage capacity. We hypothesize that in $WO_3 \cdot 2H_2O$, the structural water network restricts the phase transformation to 2D (versus 3D in WO_3), which then allows for fast proton transport within the structure. The decreased deformation of $WO_3 \cdot 2H_2O$ was also found with operando atomic force microscopy. The measurement showed that deformation during proton insertion is smaller and more reversible (lower hysteresis) when structural

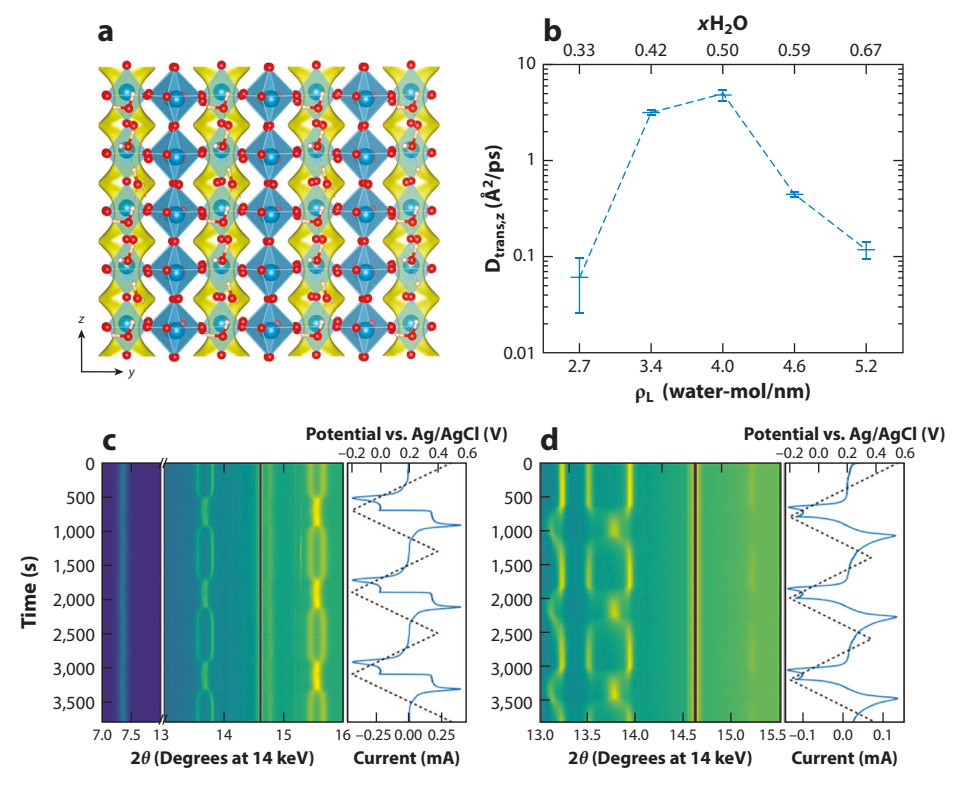


Figure 6

Proton insertion into hydrous tungsten oxides. (a) Structure of hexagonal WO₃; electron density isosurfaces (yellow) show tunnels available for 1D proton transport. (b) Calculated proton diffusivity varies as a function of the linear water density (ρ_L) controlled by the structural water content per WO₃ (xH₂O). Panels a and b adapted with permission from Reference 46; copyright 2021 American Chemical Society. (c,d) Operando synchrotron X-ray diffraction of (c) WO₃·2H₂O and (d) WO₃ during cyclic voltammetry proton insertion at 1 mV/s. Both materials undergo electrochemically induced structural transformations concomitant with proton insertion. The phase transition in the hydrous phase occurs on a faster timescale than in the anhydrous material. Panels c and d adapted with permission from Reference 34; copyright 2019 American Chemical Society.

water is present (49). First-principles DFT calculations indicate that the energetically favorable proton transport paths are along the $WO_5(OH_2)$ layers through bridging lattice oxygen, not the 2D structural water network (50), in agreement with operando XRD and inelastic neutron scattering results (34). Given the lack of interlayer spacing change during proton insertion and limited translational motion of structural water in $WO_3 \cdot 2H_2O$, we hypothesize that the structural water networks in this material stabilize the structure during electrochemical proton insertion rather than providing Grotthuss-like transport pathways. This mechanism is similar to the stabilization of TMO shear phases during Li^+ insertion (51, 52). As of now, there is no conclusive experimental evidence for the transport of inserted protons along the 2D structural water network in $WO_3 \cdot 2H_2O$. These studies of tunneled and layered hydrous tungsten oxides highlight the unique mechanisms by which structural water can enable fast proton transport and the tremendous utility of atomic-scale simulations and operando characterization in facilitating this understanding.

Hydrous RuO₂ is an oxide with unique structure and properties and whose mechanism is of significant interest to the electrochemical capacitor community (53). The seminal work by Dmowski

et al. (31) showed that hydrous RuO_2 can be viewed as a composite of rutile RuO_2 nanocrystals <10 nm in size surrounded by hydrous grain boundaries. More recent structural characterization showed that the surface is predominately hydroxylated with only a small amount of hydrogen-bound water molecules (32). The electrochemical response of hydrous RuO_2 in acidic electrolytes is almost ideally capacitive but with a high capacitance (>180 μ F/cm² of the surface) and change of the Ru oxidation state (54), both of which implicate the specific adsorption of protons and a pseudocapacitive mechanism. Recent DFT calculations show that bulk proton insertion is kinetically hindered by a large, 1.62 eV, energy barrier (55). Simulations that accounted for surface solvation and charging were quantitatively in agreement with the experimental potential versus charge profile of RuO_2 (56). This suggested the importance of the hydrous surface, as the solvent was proposed to stabilize adsorbed protons at the electrochemical interface. The facile kinetics of the proton storage process are facilitated by the hydroxylated and hydrated regions between RuO_2 clusters; experimental results show a significant decrease in the rate capability and capacitive response upon dehydration (4, 31).

As with proton insertion, structural water is proposed to enhance the kinetics of aqueous cation insertion by various mechanisms. This is of interest for energy storage with high safety and low cost (57, 58). Hydrous manganese and vanadium oxides are examples of layered hydrous TMOs that insert alkali cations at neutral pH. For example, Charles et al. (30) hypothesized that structural water provides mechanical support during K⁺ intercalation in disordered vanadium oxide nanosheets, allowing for continuous and reversible structural change over a wider potential window than in anhydrous V2O5. Intercalation of K+ can induce significant lattice strains due to its large size (1.38 Å versus 0.76 Å for Li⁺) (59), which can lead to degradation of the electrode material to accommodate the additional spatial and charge density. X-ray and neutron pair distribution function analyses were used to determine that the nanosheet structure consisted of bilayers of VO₆ octahedra separated by structural H₂O and charge-compensating intercalated K⁺. Upon cycling in an aqueous KCl electrolyte, the nanosheets exhibit a series of reversible peaks superimposed on a capacitive background. In situ XRD was used to determine the structural changes during electrochemical cycling. Intercalation of K+ was associated with a contraction of the interlayer spacing due to the Coulombic attraction of the reduced vanadium oxide layers and electrochemically intercalated K⁺. This interlayer contraction is similar to other layered hydrous TMOs, such as birnessite, undergoing cation insertion (60, 61). Comparison of fully hydrous (K_{0,22}V_{1,74}O_{4,37}·0.82H₂O) and partially hydrous (K_{0,22}V_{1,74}O_{4,15}·0.46H₂O) nanosheets showed that increased interlayer hydration led to higher specific capacity (145 mAh/g versus 103 mAh/g), rate capability, and structural stability. As a result, this study supports the hypothesis that structural water in hydrous TMOs can lead to structural stability during electrochemical ion insertion in aqueous electrolytes.

As illustrated in **Figure 1**, hydrous TMOs can exhibit large inner surface areas when structural water networks facilitate the transport of electrolyte solvent and ions to and from the bulk. Our group is interested in how ion storage changes along the continuum from solvated ion adsorption (capacitive storage with limited ion–host interaction) to desolvated ion insertion (maximum ion–host interaction that can also lead to structural transitions of the host) (62). We hypothesize that this can be tuned by the extent of confinement of the host material; **Figure 7** illustrates this as a function of the interlayer spacing in a layered host (62). Toward this goal, we investigated K⁺ intercalation from an aqueous electrolyte into birnessite, a layered hydrous TMO of interest for capacitive energy storage (60). Within an \sim 1 V potential window, birnessite exhibits a capacitive electrochemical response with the storage of \sim 0.1 e⁻/K⁺ per Mn. Using multimodal characterization and first-principles calculations, we found that K⁺ intercalation into birnessite occurs with minimal structural change (**Figure 7**b). Cyclic voltammetry and EQCM results confirmed the

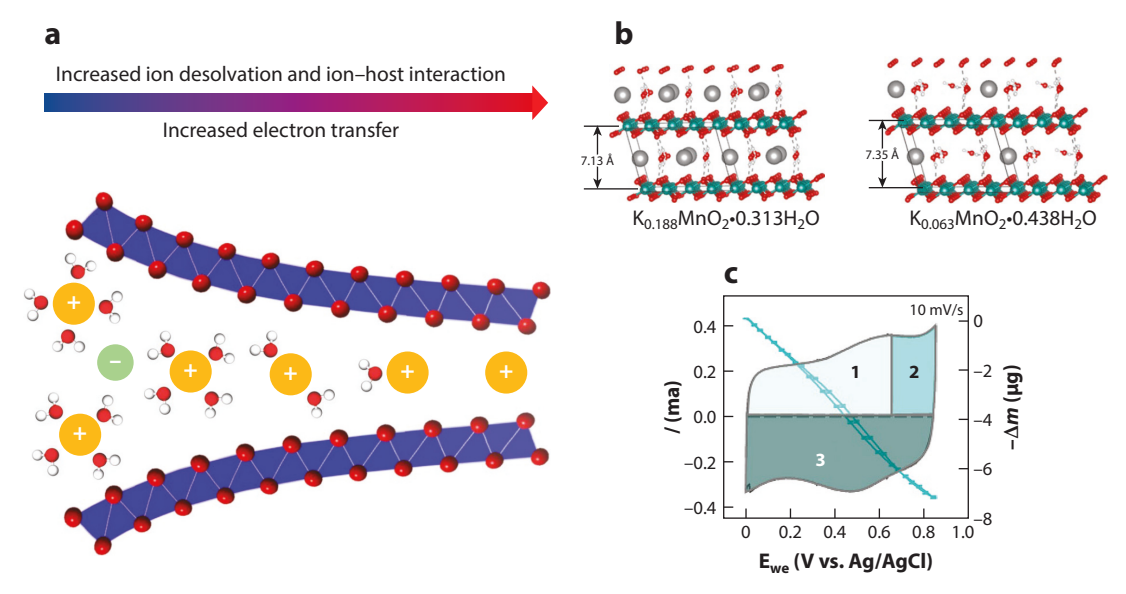


Figure 7

Role of the hydrated interlayer for cation intercalation into birnessite. (a) Conceptual diagram of how ion intercalation into a layered solid-state host changes with decreasing interlayer spacing, from adsorption at the outer surface (limited ion–host interaction) to intercalation of a desolvated cation (maximum ion–host interaction). (b) Density-functional theory (DFT) structures and composition of birnessite in the intercalated and deintercalated states, showing change in interlayer spacing and K^+ and structural water content. (c) Cyclic voltammetry and mass change versus potential of birnessite in a K_2SO_4 electrolyte showing low hysteresis and three distinct regions (labeled 1, 2, and 3) that correspond to different mass-to-charge ratios. The total mass change is lower than if charge storage were due only to K^+ , indicating the involvement of other species such as structural water, in agreement with the DFT calculations. Panel a adapted with permission from Reference 62. Panels b and c adapted with permission from Reference 60.

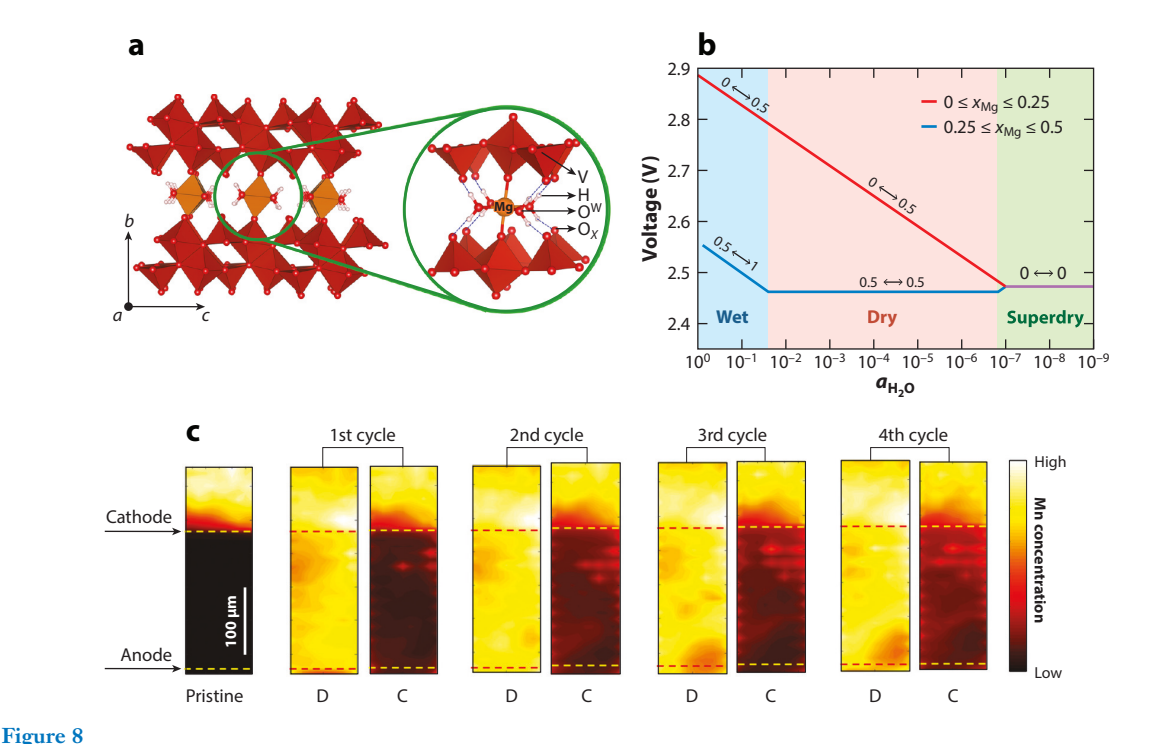
involvement of K^+ as well as water molecules in the insertion mechanism (**Figure 7***c*). Follow-on work with buffered electrolytes indicated that protons do not participate in the capacitive storage mechanism and instead lead to dissolution of the birnessite over time (5). On the basis of these results, we hypothesize that K^+ intercalation into birnessite appears capacitive because the mechanism occurs with minimal interaction between K^+ and the manganese oxide layers. In effect, the mechanism operates as depicted on the left side of **Figure 7***a*, with structural water molecules again leading to increased structural stability and partial hydration of the intercalated K^+ within the interlayer. This hypothesis is supported by ReaxFF reactive force field–based MD and grand canonical Monte Carlo simulations that show intercalated K^+ resides in the middle of the interlayer surrounded by water molecules.

Cation insertion into hydrous TMOs has also been investigated in nonaqueous electrolytes. In a nonaqueous environment, the stability of the structural water needs to be carefully considered as its loss can lead to structural change of the oxide and/or contamination of the nonaqueous electrolyte. Experimental results indicate two extremes for the role of structural water during cation insertion from a nonaqueous electrolyte: (a) improvement of insertion kinetics, as in aqueous electrolytes, or (b) formation of irreversible products such as hydroxide salts and electrolyte contamination. In the case of a beneficial response, we found that WO₃·H₂O exhibits faster Li⁺ insertion than WO₃; the interlayer water of WO₃·2H₂O is not stable in a nonaqueous electrolyte (63). Electrochemical Li⁺ insertion into WO₃·H₂O can occur over a wider potential window, which we hypothesized was due to fewer structural transitions taking place in WO₃·H₂O versus WO₃. Using EQCM, we found that Li⁺ insertion does not involve solvent coinsertion in

 $WO_3 \cdot H_2O$ and WO_3 . Electrochemical impedance spectroscopy results showed that charge storage in $WO_3 \cdot H_2O$ persists to higher frequencies and with lower time constants over a broader potential range than in WO_3 , supporting the hypothesis that structural water leads to more reversible Li^+ insertion. Conversely, structural water was found to inhibit Li^+ insertion from a nonaqueous electrolyte into V_2O_5 aerogels ($V_2O_5 \cdot 0.6H_2O$) (23). The aerogel structure consists of a vanadium oxide bilayer separated by an interlayer containing structural water molecules. When reduced to 1.5 V versus Li/Li^+ , V_2O_5 aerogels can store up to 2 Li^+ per V, leading to an attractive capacity of 320 mAh/g. However, the capacity declines to about half of its initial value by 35 cycles. XPS of the cycled aerogel showed accumulation of LiOH, which is electrochemically inactive. As a result, in the case of deep cycling of V_2O_5 aerogels, the reactivity of structural water with Li^+ is hypothesized to limit the cycling stability.

Hydrous TMOs are of interest for multivalent cation insertion. Energy storage devices based on multivalent cations such as Mg²⁺ or Zn²⁺ may lead to higher energy densities and better sustainability than those based on Li+ (64). Multivalent cation insertion can occur from either aqueous or nonaqueous electrolytes, and hydrous TMOs have been used as insertion hosts in both systems. Due to the high charge-to-mass ratio of multivalent cations as compared with monovalent cations, their insertion kinetics are considered more sluggish (65). The slow kinetics can arise from multiple factors, including high interfacial desolvation energy and slow solid-state transport (66). Structural water is hypothesized to enable fast multivalent cation insertion via several proposed mechanisms: (a) allowing for solvent coinsertion into the large interlayer or tunnel spaces pillared by structural water molecules and (b) serving as a shield between the intercalated cations and the oxide host (66-68). For example, our work on the insertion of Mg²⁺ from a nonaqueous electrolyte into hydrated WO3 indeed showed faster insertion kinetics, though decreased specific capacity, in WO₃·H₂O as compared with WO₃ (69). Structural water was shown to enhance insertion kinetics in layered manganese oxides in nonaqueous Mg²⁺ and aqueous Zn²⁺ electrolytes (70, 71). Xerogel V₂O₅ nH₂O can reversibly intercalate up to 0.25 Mg²⁺ per V₂O₅ from a nonaqueous, 1 M Mg(TFSI)₂ diglyme electrolyte (72). The interlayer spacing of the xerogel V₂O₅ contracts upon Mg²⁺ intercalation. DFT calculations of V₂O₅ xerogel intercalated with Mg²⁺ showed that water cointercalation from a wet, nonaqueous electrolyte led to higher voltages than when no water was present (73), suggesting that structural water promotes multivalent cation insertion. The predicted structure of the intercalated xerogel showed Mg2+ coordinated by two lattice oxygens and four oxygens from structural water molecules in the interlayer (Figure 8a). The water content of the electrolyte was found to control the amount of cointercalated H₂O, and the insertion voltage was calculated to be 150 mV higher in a wet versus dry electrolyte (Figure 8b). A favorable interlayer environment for multivalent cation intercalation was also found in $Zn_{0.25}V_2O_5$. nH_2O_5 , which was proposed as a high-capacity cathode for aqueous Zn batteries (41). The hypothesized intercalation mechanism involved countermovements of Zn²⁺ and water molecules to explain the structural stability and rate capability in a 1 M ZnSO₄ electrolyte. These results all suggest a beneficial role of structural water for multivalent electrochemical cation insertion. However, there are additional considerations when evaluating the behavior of hydrous TMOs for multivalent cation insertion.

Recent results indicate that the role of structural water during multivalent cation insertion may be even more complex due to the possibility of multiple reaction mechanisms involving protons and water molecules (74, 75). This is especially the case in aqueous electrolytes since multivalent cations such as Mg²⁺, Al³⁺, and Zn²⁺ are Lewis acids that can accept electrons from water molecules, leading to an increase in [H⁺] and a lower pH. As a result, in multivalent cation aqueous electrolytes or nonaqueous electrolytes containing additional water, the charge storage mechanism may primarily be due to proton insertion or even involve proton-driven



Reactivity of hydrous TMOs in electrolytes containing multivalent cations. (a) Calculated structure of $Mg_{0.25}V_2O_5 \cdot H_2O$ xerogel with intercalated Mg^{2+} residing in the interlayer and octahedrally coordinated by terminal oxygens (O_x) and structural water oxygens (O^W) . (b) Calculated variation in the insertion voltage for Mg^{2+} into a V_2O_5 xerogel based on the water content (a_{H_2O}) of the nonaqueous electrolyte; more water leads to higher insertion voltages. (c) X-ray fluorescence map of Mn during cycling of α -MnO₂ in an aqueous ZnSO₄ electrolyte. The concentration of Mn in the electrolyte increases with cycling, which is attributed to a dissolution/deposition mechanism involving dissolved Mn (and not Zn²⁺ insertion into α -MnO₂). Panels a and b adapted with permission from Reference 73; copyright 2016 American Chemical Society. Panel c adapted with permission from Reference 77.

dissolution/reprecipitation reactions. For example, V_2O_5 nanorods cycled in an $Al(OTf)_3$ aqueous electrolyte with pH=2 were shown to insert only protons and not Al^{3+} (76).

An example of dissolution/reprecipitation reactions upon cycling in an aqueous electrolyte containing multivalent cations occurs with $\alpha\text{-MnO}_2$ ($K_{0.97}Mn_8O_{16}\cdot 0.56H_2O$), a hydrous TMO with tunnels containing structural water and cations (77). Given its open structure, the charge storage mechanism of $\alpha\text{-MnO}_2$ in Zn^{2+} aqueous electrolytes was hypothesized to involve Zn^{2+} insertion, perhaps facilitated by the structural water in the tunnels, as discussed in Section 2. However, operando X-ray fluorescence measurements (**Figure 8**c) showed that the charge storage mechanism does not involve a solid-state insertion, or even conversion, reaction. Instead, the mechanism involved dissolution of Mn^{2+} during reduction of $\alpha\text{-MnO}_2$, followed by deposition of a zinc-containing tunnel oxide during oxidation with a composition of $ZnMn_3O_7\cdot 3H_2O$. This result showed the importance of operando measurements to determine the mechanism, since the final structure was a Zn-containing tunnel manganese oxide as might be obtained via solid-state insertion. The detection of dissolved Mn species in the electrolyte and their increase during cycling allowed for the discovery of the dissolution/deposition mechanism. This mechanism should be considered whenever oxide materials exhibit high specific capacities (especially >1 e^- per transition metal) in aqueous electrolytes.

4. ELECTROCHEMICAL ENERGY CONVERSION

Electrochemical energy conversion reactions in aqueous electrolytes, such as hydrogen and oxygen evolution reactions in water splitting, expose electrocatalysts to harsh chemical environments and highly reducing or oxidizing potentials. As a result, the properties of TMO electrocatalysts are dynamic (78) and depend on the properties of the electrochemical environment at a given point in time, such as the interfacial pH, concentration, potential, and state of charge. Such conditions can lead to the formation of hydrous TMOs that serve as the true electrochemically active phase in electrochemical energy conversion reactions.

Hydrous nickel and cobalt hydroxides are some of the most actively studied materials for electrochemical water splitting due to their low cost and high activity for the oxygen evolution reaction (OER) in alkaline electrolytes (79, 80). These hydrous TMOs have been termed electrolyte-permeable catalysts because their catalytic activity involves the entire volume of the material, that is, the inner surface (**Figure 9**). (81) The dynamic nature of the composition of β -Co(OH)₂ during OER was studied with operando scanning probe and X-ray microscopies (82). Prior to the onset of the OER, single crystalline platelets of β -Co(OH)₂ transform to a protonated and hydrous structure, α -Co(OH)₂H_{1.5}·0.5H₂O. At higher voltages, the protons and structural water deintercalate to form β -CoOOH. The scanning probe and X-ray microscopy techniques also provided insight into the spatial distribution of the phase transitions, which were heterogeneous over the bulk of the particles. Correlation between the Co³⁺ concentration at particle edges and the Tafel slope led to the conclusion that the local composition driven by bulk ion and water movement was responsible for changes in the electrocatalytic activity of the material as a function of potential. These studies highlight the significance of facile proton, cation, and water transport in hydrous TMOs for both electrochemical energy storage and conversion applications.

Another tantalizing feature of some hydrous TMOs is that their interlayer composition can be varied during synthesis in order to improve electrocatalytic activity. One example of this occurs with birnessite, which is of interest as a low-cost catalyst for the OER. Exfoliated birnessite nanosheets can be stacked into bilayers with different hydrated, chemically intercalated interlayer

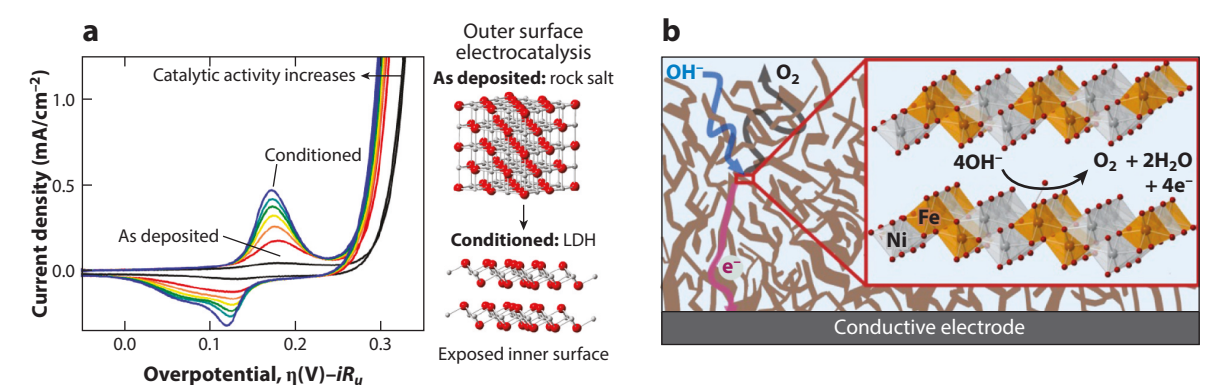


Figure 9

Formation of hydrous transition metal oxides (TMOs) from dense TMO electrocatalysts in an aqueous electrolyte. Electrochemical conditions during aqueous energy conversion reactions can promote the formation of hydrous TMOs that can exhibit high specific activity. (a) Evolution of a NiO electrocatalyst during the oxygen evolution reaction in an aqueous KOH electrolyte. Electrocatalytic activity increases when the original rock salt structure of NiO transforms to a hydrous layered double hydroxide (LDH). The LDH is hypothesized to provide an inner surface for electrochemical reactivity via the hydrous interlayer. (b) Schematic of the electrolyte-permeable electrode inner surface due to the formation of hydrous LDH from bulk NiO. The open disordered framework is hypothesized to facilitate electrolyte transport and the number of electrocatalytic active sites. Figure adapted with permission from Reference 79; copyright 2015 American Chemical Society.

cations. An experimental study found a correlation between the OER overpotential and the interlayer spacing of birnessite (determined by the type of alkali cation in the interlayer), with the largest interlayer spacing (Cs⁺) leading to the lowest overpotential (83). The confinement of charge-compensating transition metal cations such as nickel and cobalt in the interlayer of birnessite also leads to higher OER activity (300-400 mV lower overpotentials at 10 mA/cm²) (84, 85). First-principles calculations show that the interlayer cation speciation in birnessite determines the manganese oxidation state (Mn^{3+/4+}) and ordering, which affect the electronic properties of the material (86). First-principles simulations indicate that the electronic structure formed from the interactions of manganese oxide sheets with differing Mn³⁺ content facilitates electron transfer between the oxide and intercalated species, enhancing O₂ production rates (87). This result further suggests that a nonuniform distribution of Mn³⁺ favors high OER activity in birnessite. This understanding was used to synthesize birnessite with alternating low and high Mn³⁺ content layers with intercalated Cs⁺, which led to a decrease of the OER overpotential by 250 mV as compared with unmodified birnessite with K⁺ in the interlayer (88). Finally, MD simulations indicate that structural water within the interlayer of birnessite exhibits geometric frustration, which was proposed to facilitate electrocatalysis by lowering the Marcus reorganization energy for electron transfer (89). These comprehensive investigations demonstrate how the hydrous inner surface environment can be tuned for electrochemical reactivity in hydrous TMOs.

Hydrous TMOs can form when anhydrous TMOs are used as electrocatalysts in aqueous electrolytes driven by chemical dissolution/reprecipitation or proton exchange accompanied by structural water molecules. For example, oxidation of α-Li₂IrO₃ in an aqueous electrolyte occurs with Li⁺ deintercalation and the formation of a birnessite-like phase, where the interlayer contains Li⁺, K⁺, and structural water (Figure 10a,b). The layered hydrous phase is electrocatalytically active toward the OER, and O₂ evolution is linearly dependent on the K⁺ content in the interlayer (Figure 10c), indicating the modulation of electrocatalytic behavior based on the interlayer alkali content and state of charge of the hydrous phase. The proposed electrocatalytic mechanism (Figure 10d) highlights the dynamic nature of the electrolyte and the key role of structural water in enabling access to the inner surface of the TMO for K⁺ intercalation from the aqueous electrolyte. Another example of the importance of a hydrous phase for OER catalysis is the protonation of Sr₂IrO₄ to yield a hydrous phase, H_{3.6}IrO₄·3.7H₂O, which exhibits higher OER activity than the parent material (6). Our group also studied the importance of the dynamic modulation of hydrated phase properties during electrocatalysis in tungsten oxide hydrates (90). We synthesized an octylamine-pillared WO₃ (OA-WO₃) from WO₃·H₂O; OA-WO₃ contained octylamine in the interlayer as opposed to structural water. Unlike WO₃·H₂O, the octylamine-saturated interlayer of OA-WO₃ did not allow proton or alkali cation insertion. We found a correlation between proton insertion into tungsten oxides and the hydrogen evolution reaction (HER) activity: Higher proton insertion (as in WO₃·H₂O) led to lower overpotential for the HER. This provides further evidence of the importance of understanding the role of proton or cation insertion into hydrous oxides used in aqueous electrocatalysis.

5. ENVIRONMENTAL APPLICATIONS OF HYDROUS TRANSITION METAL OXIDES

The specificity of ion insertion into solid-state hosts, including hydrous TMOs, can be used in emerging environmental technologies including electrochemical ion separation and recovery (92, 93). This includes such aqueous electrolyte, ion-based processes as electrochemical desalination (uptake of Na⁺ and Cl⁻), water treatment (removal of toxic elements, e.g., Cr⁶⁺), and element recovery (e.g., Li⁺). While activated carbon–based electrodes are the most commonly used materials for these applications, hydrous TMOs can exhibit higher ion specificity and removal capacities due

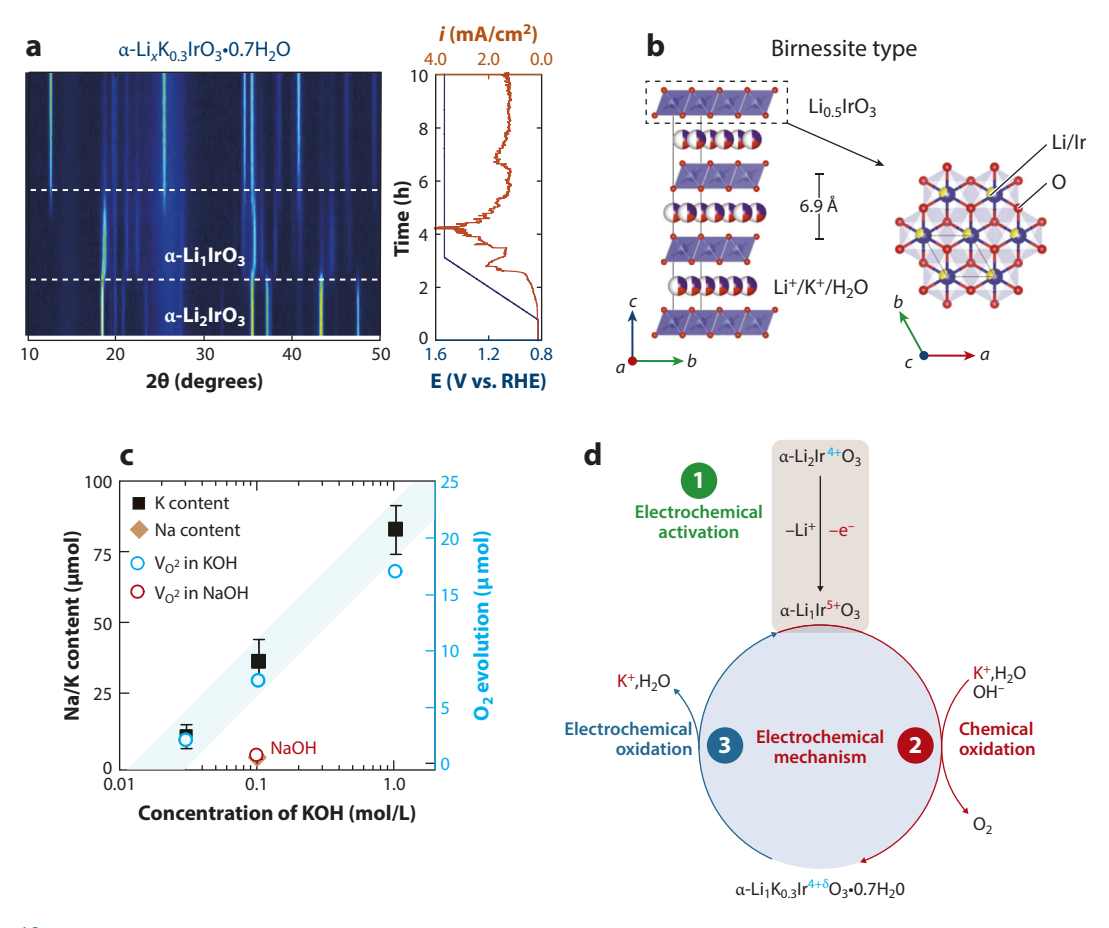


Figure 10

Evolution of a transition metal oxide (TMO) into a hydrous TMO with high oxygen evolution reaction activity. (a) Operando X-ray diffraction of α -Li₂IrO₃ during electrochemical oxidation in a KOH electrolyte: a hydrous, birnessite-like phase forms during the potential hold at 1.55 V versus reversible hydrogen electrode (RHE). (b) Structural model of electrochemically formed α -Li_xK_{0.3}IrO₃·0.7H₂O. (c) Correlation between the intercalation of K⁺ into the hydrous TMO and O₂ gas evolution. (d) Proposed mechanism involving the formation of a hydrous TMO. Figure adapted with permission from Reference 91.

to bulk insertion. Hydrous TMOs are most suitable for the removal of small cations because their interlayers are typically not vacant enough for larger electrolyte species. For example, hydrated layered and tunnel manganese oxides were studied for their ability to insert Na⁺ from aqueous electrolytes (94, 95). In the case of tunnel manganese oxides, larger tunnel size was associated with the removal of cations with larger hydrated radii, such as Mg^{2+} (95). This suggests that manganese oxide tunnel size may be tuned for cation removal selectivity. In layered manganese oxides, both birnessite and buserite demonstrated high initial Na⁺ removal, but long-term cycling led to a decline of the removal capacity due to disorder of the layered structure. The large interlayer spacing of both structures contained high amounts of structural water, which was correlated with more facile mobility of the aqueous cations. The degree of ion uptake by manganese oxides is strongly influenced by their crystallinity and microstructure and the microenvironment of the interlayer or tunnel spaces (96, 97). Jin et al. (98) found that lamellar, poorly crystalline MnO_2 exhibited higher salt adsorption capacity than more crystalline manganese oxides. Hydrous V_2O_5

Chemical Society.

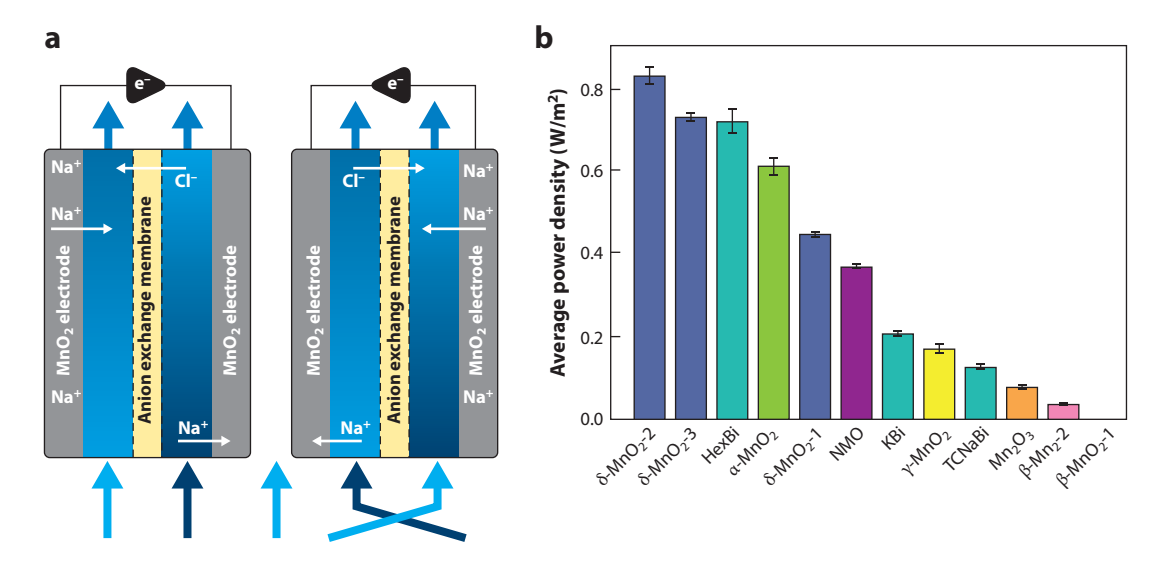


Figure 11

Hydrous transition metal oxides for harvesting salinity gradient energy. (a) Schematic of a salinity gradient flow cell utilizing symmetric manganese oxide electrodes; the water flow was alternated between two paths (stage 1 and stage 2). (b) Comparison of the average power density of different manganese oxide electrodes. Figure adapted with permission from Reference 100; copyright 2020 American

has also been studied for desalination, showing good Na⁺ uptake via cation intercalation into the hydrated interlayer (99). Another environmental application of hydrous TMOs is as electrodes in salinity gradient energy harvesting, a process that is the opposite of desalinization (100). Manganese oxide electrodes are used for the reversible insertion of Na⁺ from water with both high and low concentrations of NaCl (**Figure 11a**). Based on power density, hydrous manganese oxides capable of Na⁺ intercalation showed the best performance (**Figure 11b**). Given the importance of hydrous TMO minerals such as birnessite in scavenging metal ions from soils (101), research into the use of hydrous TMOs for electrochemical environmental applications is likely to increase in the future, particularly with improvements in their specificity of ion insertion.

6. CONCLUSIONS

Hydrous TMOs are solid-state materials, the inner surface of which can be accessible for electrochemical reactivity. They are of interest as electrodes for insertion-type energy storage, electrocatalysts, and environmental applications. The possibility of tuning the inner surface environment of hydrous TMOs and the interesting physicochemical properties of water under confinement by these materials are drivers for scientific studies into this class of materials. From a technological perspective, they are important for a variety of energy and environmental technologies, particularly in aqueous electrolytes. Further advancements in controlling the composition and specificity of ion uptake and mass transport kinetics of hydrous TMOs will lead to further applications of these materials in electrochemical energy storage, conversion, and environmental remediation.

DISCLOSURE STATEMENT

The authors are not aware of any affiliations, memberships, funding, or financial holdings that might be perceived as affecting the objectivity of this review.

ACKNOWLEDGMENTS

We thank our current and former group members and collaborators for many useful discussions on hydrous TMOs for electrochemical energy and environmental applications. A portion of the research described in this review used the backscattering spectrometer BASIS at the Spallation Neutron Source, a Department of Energy (DOE) Office of Science User Facility operated by Oak Ridge National Laboratory. Oak Ridge National Laboratory is managed by UT-Battelle, LLC, for the US DOE under contract DEAC05-00OR22725. This review is based upon work supported by the National Science Foundation under grant DMR-1653827.

Erratum >

LITERATURE CITED

- Ardizzone S, Fregonara G, Trasatti S. 1990. "Inner" and "outer" active surface of RuO₂ electrodes. Electrochim. Acta 35:263-67
- Burke LD, Lyons MEG. 1986. Electrochemistry of hydrous oxide films. In Modern Aspects of Electrochemistry, No. 18, ed. RE White, JO Bockris, BE Conway, pp. 169–248. New York: Plenum
- 3. Freedman ML. 1959. The tungstic acids. 7. Am. Chem. Soc. 81(15):3834-39
- Zheng JP, Cygan PJ, Jow TR. 1995. Hydrous ruthenium oxide as an electrode material for electrochemical capacitors. J. Electrochem. Soc. 142(8):2699–703
- Saeed S, Fortunato J, Ganeshan K, van Duin ACT, Augustyn V. 2021. Decoupling proton and cation contributions to capacitive charge storage in birnessite in aqueous electrolytes. *ChemElectroChem* 8(22):4371–79
- Zhang R, Pearce PE, Pimenta V, Cabana J, Li H, et al. 2020. First example of protonation of Ruddlesden– Popper Sr₂IrO₄: a route to enhanced water oxidation catalysts. *Chem. Mater.* 32(8):3499–509
- Hall DS, Lockwood DJ, Bock C, MacDougall BR. 2015. Nickel hydroxides and related materials: a review of their structures, synthesis and properties. Proc. R. Soc. A 471:20140792
- 8. Jha G, Tran T, Qiao S, Ziegler JM, Ogata AF, et al. 2018. Electrophoretic deposition of mesoporous niobium(V)oxide nanoscopic films. *Chem. Mater.* 30(18):6549–58
- Pensel A, Peulon S. 2018. In situ XANES measurements during electrodeposition of thin film: example
 of birnessite, a promising material for environmental applications. *Electrochim. Acta* 281:738–45
- Schaak RE, Mallouk TE. 2002. Exfoliation of layered rutile and perovskite tungstates. Chem. Commun. 2(7):706–7
- Wang R, Sun Y, Brady AB, Fleischmann S, Eldred TB, et al. 2021. Fast proton insertion in layered H₂W₂O₇ via selective etching of an aurivillius phase. Adv. Energy Mater. 11(1):2003335
- Lemaire P, Sel O, Alves Dalla Corte D, Iadecola A, Perrot H, Tarascon J-MM. 2020. Elucidating the origin of the electrochemical capacity in a proton-based battery H_xIrO₄ via advanced electrogravimetry. ACS Appl. Mater. Interfaces 12(4):4510–19
- 13. Rao RR, Tułodziecki M, Han B, Risch M, Abakumov A, et al. 2020. Reactivity with water and bulk ruthenium redox of lithium ruthenate in basic solutions. *Adv. Funct. Mater.* 31(2):2002249
- Buchholz D, Chagas LG, Vaalma C, Wu L, Passerini S. 2014. Water sensitivity of layered P2/P3-Na_xNi_{0.22}Co_{0.11}Mn_{0.66}O₂ cathode material. *J. Mater. Chem. A.* 2(33):13415–21
- Boyd S, Dhall R, LeBeau JM, Augustyn V. 2018. Charge storage mechanism and degradation of P2-type sodium transition metal oxides in aqueous electrolytes. 7. Mater. Chem. A. 6(44):22266–76
- Daniel MF, Desbat B, Lassegues JC, Gerand B, Figlarz M. 1987. Infrared and Raman study of WO₃ tungsten trioxides and WO₃, xH₂O tungsten trioxide hydrates. J. Solid State Chem. 67(2):235–47
- Birkner N, Navrotsky A. 2017. Thermodynamics of manganese oxides: sodium, potassium, and calcium birnessite and cryptomelane. PNAS 114(7):E1046–53
- 18. Szymański JT, Roberts AC. 1984. The crystal structure of tungstite, WO₃-H₂O. Can. Mineral. 22:681–88
- Crouch-Baker S, Dickens PG. 1984. The deuterium-atom positions in deuterated molybdic acid, MoO₃·2D₂O, by powder neutron diffraction. *Acta Crystallogr. C* 40(7):1121–24
- Mitchell JB, Lo WC, Genc A, LeBeau J, Augustyn V. 2017. Transition from battery to pseudocapacitor behavior via structural water in tungsten oxide. *Chem. Mater.* 29(9):3928–37

- Wang R, Chung C, Liu Y, Jones JL, Augustyn V. 2017. Electrochemical intercalation of Mg²⁺ into anhydrous and hydrated crystalline tungsten oxides. *Langmuir* 33(37):9314–23
- Kattouf B, Frey GL, Siegmann A, Ein-Eli Y. 2009. Enhanced reversible electrochromism via in situ phase transformation in tungstate monohydrate. Chem. Commun. 2009(47):7396–98
- Wangoh LW, Huang Y, Jezorek RL, Kehoe AB, Watson GW, et al. 2016. Correlating lithium hydroxyl accumulation with capacity retention in V₂O₅ aerogel cathodes. ACS Appl. Mater. Interfaces 8:11532–38
- Chen D, Li T, Yin L, Hou X, Yu X, et al. 2011. A comparative study on reactions of n-alkylamines with tungstic acids with various W–O octahedral layers: novel evidence for the "dissolution-reorganization" mechanism. *Mater. Chem. Phys.* 125(3):838–45
- Kittaka S, Hamaguchi H, Shinno T, Takenaka T. 1996. Interlayer water molecules in the vanadium pentoxide hydrate, V₂O₅·nH₂O. 6. Rigidity of crystal structure against water adsorption and anisotropy of electrical conductivity. *Langmuir* 12(4):1078–83
- Takahara S, Kittaka S, Kuroda Y, Yamaguchi T, Fujii H, Bellissent-Funel M-C. 2000. Interlayer water molecules in vanadium pentoxide hydrate, V₂O₅·nH₂O. 7. Quasi-elastic neutron scattering study. Langmuir 16:10559–63
- 27. Uchida N, Kittaka S. 1994. Interlayer water molecules in vanadium pentoxide hydrate, V₂O₅·nH₂O. 5. Dynamic motion analyzed by impedance measurements. *J. Phys. Chem.* 98(8):2129–33
- Aldebert P, Baffier N, Gharbi N, Livage J. 1981. Layered structure of vanadium pentoxide gels. Mater. Res. Bull. 16(6):669–76
- Kittaka S, Uchida N, Kihara T, Suetsugi T, Sasaki T. 1992. Interlayer water molecules in vanadium pentaoxide hydrate.
 Effect of intercalated metal ions on the adsorbability of water molecules. *Langmuir* 8(1):245–48
- Charles DS, Feygenson M, Page K, Neuefeind J, Xu W, Teng X. 2017. Structural water engaged disordered vanadium oxide nanosheets for high capacity aqueous potassium-ion storage. Nat. Commun. 8:15520
- Dmowski W, Egami T, Swider-Lyons KE, Love CT, Rolison DR. 2002. Local atomic structure and conduction mechanism of nanocrystalline hydrous RuO₂ from X-ray scattering. J. Phys. Chem. B. 106(49):12677–83
- 32. Parker SF, Robertson SJ, Imberti S. 2019. Structure and spectroscopy of the supercapacitor material hydrous ruthenium oxide, RuO₂·xH₂O, by neutron scattering. *Mol. Phys.* 117(22):3417–23
- 33. De Graef M, McHenry ME. 2012. Structure of Materials. Cambridge, UK: Cambridge Univ. Press. 2nd ed.
- Mitchell JB, Geise NR, Paterson AR, Osti NC, Sun Y, et al. 2019. Confined interlayer water promotes structural stability for high-rate electrochemical proton intercalation in tungsten oxide hydrates. ACS Energy Lett. 4:2805–12
- Kang S, Reeves KG, Aguilar I, Porras Gutierrez AG, Badot JC, et al. 2021. Ordering of a nanoconfined water network around zinc ions induces high proton conductivity in layered titanate. *Chem. Mater.* 34(9):3967–75
- Hu X, Kitchaev DA, Wu L, Zhang B, Meng Q, et al. 2018. Revealing and rationalizing the rich polytypism of todorokite MnO₂. 7. Am. Chem. Soc. 140(22):6961–68
- 37. Yuan Y, Liu C, Byles BW, Yao W, Song B, et al. 2019. Ordering heterogeneity of [MnO₆] octahedra in tunnel-structured MnO₂ and its influence on ion storage. *Joule* 3(2):471–84
- 38. Lalik E, Drużbicki K, Irvine G, Gutmann M, Rudić S, et al. 2021. Interplay between local structure and nuclear dynamics in tungstic acid: a neutron scattering study. *J. Phys. Chem. C.* 125(43):23864–79
- Lan J, Iannuzzi M. 2022. Nuclear quantum effects at aqueous metal interfaces captured by molecular dynamics simulations. Curr. Opin. Electrochem. 33:100934
- Whittingham MS. 2000. Insertion electrodes as SMART materials: the first 25 years and future promises. Solid State Ionics 134(1–2):169–78
- 41. Kundu D, Adams BD, Duffort V, Vajargah SH, Nazar LF. 2016. A high-capacity and long-life aqueous rechargeable zinc battery using a metal oxide intercalation cathode. *Nat. Energy* 1:16119
- 42. Ji X. 2019. A paradigm of storage batteries. Energy Environ. Sci. 12:3203-24
- 43. Liang G, Mo F, Ji X, Zhi C. 2021. Non-metallic charge carriers for aqueous batteries. *Nat. Rev. Mater.* 6:109–23

- Kang S, Singh A, Reeves KG, Badot J-C, Durand-Vidal S, et al. 2020. Hydronium ions stabilized in a titanate-layered structure with high ionic conductivity: application to aqueous proton batteries. *Chem. Mater.* 32(21):9458–69
- 45. Jiang H, Hong JJ, Wu X, Surta TW, Qi Y, et al. 2018. Insights on the proton insertion mechanism in the electrode of hexagonal tungsten oxide hydrate. *J. Am. Chem. Soc.* 140(37):11556–59
- Sun Y, Zhan C, Kent PRC, Jiang DE. 2021. Optimal linear water density for proton transport in tunnel oxides. J. Phys. Chem. C. 125(21):11508–12
- Judeinstein P, Livage J. 1989. Role of the water content on the electrochromic properties of WO₃, nH₂O thin films. *Mater. Sci. Eng. B* 3:129–32
- 48. Fleischmann S, Mitchell JB, Wang R, Zhan C, Jiang D, et al. 2020. Pseudocapacitance: From fundamental understanding to high power energy storage materials. *Chem. Rev.* 120(14):6738–82
- Wang R, Mitchell JB, Gao Q, Tsai WY, Boyd S, et al. 2018. Operando atomic force microscopy reveals mechanics of structural water driven battery-to-pseudocapacitor transition. ACS Nano 12(6):6032–39
- Lin H, Zhou F, Liu C-PP, Ozoliņš V. 2014. Non-Grotthuss proton diffusion mechanism in tungsten oxide dihydrate from first-principles calculations. J. Mater. Chem. A. 2(31):12280–88
- Griffith KJ, Wiaderek KM, Cibin G, Marbella LE, Grey CP. 2018. Niobium tungsten oxides for highrate lithium-ion energy storage. Nature 559(7715):556–63
- 52. Cava RJ, Murphy DW, Zahurak S. 1983. Lithium insertion in Wadsley-Roth phases based on niobium oxide. 7. Electrochem. Soc. 130(12):2345–51
- Conway BE. 1999. The electrochemical behavior of ruthenium oxide as a material for electrochemical capacitors. In *Electrochemical Supercapacitors: Scientific Fundamentals and Technological Applications*, pp. 259– 97. New York: Springer
- Mo Y, Antonio MR, Scherson DA. 2000. In situ Ru K-edge X-ray absorption fine structure studies of electroprecipitated ruthenium dioxide films with relevance to supercapacitor applications. J. Phys. Chem. B. 104(42):9777–79
- Ozolins V, Zhou F, Asta M. 2013. Ruthenia-based electrochemical supercapacitors: insights from firstprinciples calculations. Acc. Chem. Res. 46(5):1084–93
- Keilbart N, Okada Y, Dabo I. 2019. Probing the pseudocapacitance and energy-storage performance of RuO₂ facets from first principles. *Phys. Rev. Mater.* 3(8):85405
- Boyd S, Augustyn V. 2018. Transition metal oxides for aqueous sodium-ion electrochemical energy storage. *Inorg. Chem. Front.* 5(5):999–1015
- 58. Kim H, Hong J, Park KY, Kim H, Kim SW, Kang K. 2014. Aqueous rechargeable Li and Na ion batteries. *Chem. Rev.* 114(23):11788–827
- Shannon RD. 1976. Revised effective ionic radii and systematic studies of interatomic distances in halides and chalcogenides. Acta Crystallogr. A 32(5):751–67
- Boyd S, Ganeshan K, Tsai W-Y, Wu T, Saeed S, et al. 2021. Effects of interlayer confinement and hydration on capacitive charge storage in birnessite. Nat. Mater. 20:1689–94
- Shan X, Guo F, Charles DS, Lebens-Higgins Z, Abdel Razek S, et al. 2019. Structural water and disordered structure promote aqueous sodium-ion energy storage in sodium-birnessite. *Nat. Commun.* 10(1):4975
- 62. Fleischmann S, Zhang Y, Wang X, Cummings PT, Wu J, et al. 2022. Continuous transition from double-layer to Faradaic charge storage in confined electrolytes. *Nat. Energy* 7(3):222–28
- Mitchell JB, Wang R, Ko JS, Long JW, Augustyn V. 2022. Critical role of structural water for enhanced Li⁺ insertion kinetics in crystalline tungsten oxides. *J. Electrochem. Soc.* 169(3):030534
- Muldoon J, Bucur CB, Gregory T. 2014. Quest for nonaqueous multivalent secondary batteries: magnesium and beyond. Chem. Rev. 114:11683–720
- 65. Yoo HD, Shterenberg I, Gofer Y, Gershinsky G, Pour N, Aurbach D. 2013. Mg rechargeable batteries: an on-going challenge. *Energy Environ. Sci.* 6(8):2265–79
- Levi E, Gofer Y, Aurbach D. 2010. On the way to rechargeable Mg batteries: the challenge of new cathode materials. Chem. Mater. 22(3):860–68
- 67. Novák P, Scheifele W, Joho F, Haas O. 1995. Electrochemical insertion of magnesium into hydrated vanadium bronzes. *7. Electrochem. Soc.* 142(8):2544–50

- Lee HJ, Shin J, Choi JW. 2018. Intercalated water and organic molecules for electrode materials of rechargeable batteries. Adv. Mater. 30(42):1705851
- Wang R, Chung C-C, Liu Y, Jones JL, Augustyn V. 2017. Electrochemical intercalation of Mg²⁺ into anhydrous and hydrated crystalline tungsten oxides. *Langmuir* 33(37):9314–23
- Nam KW, Kim S, Lee S-SS, Salama M, Shterenberg I, et al. 2015. The high performance of crystal water containing manganese birnessite cathodes for magnesium batteries. Nano Lett. 15:4071–79
- Nam KW, Kim H, Choi JH, Choi JW. 2019. Crystal water for high performance layered manganese oxide cathodes in aqueous rechargeable zinc batteries. Energy Environ. Sci. 12(6):1999–2009
- 72. Sa N, Kinnibrugh L, Wang H, Gautam GS, Chapman KW, et al. 2016. Structural evolution of reversible Mg insertion into a bilayer structure of V₂O₅·nH₂O xerogel material. *Chem. Mater.* 28(9):2962–69
- Sai Gautam G, Canepa P, Richards WD, Malik R, Ceder G. 2016. Role of structural H₂O in intercalation electrodes: the case of Mg in nanocrystalline xerogel-V₂O₅. Nano Lett. 16(4):2426–31
- Johnston B, Henry H, Kim N, Lee SB. 2021. Mechanisms of water-stimulated Mg²⁺ intercalation in vanadium oxide: toward the development of hydrated vanadium oxide cathodes for mg batteries. Front. Energy Res. 8:611391
- Lopez M, Yoo HD, Hu L, Andrews JL, Banerjee S, Cabana J. 2020. Does water enhance Mg intercalation in oxides? The case of a tunnel framework. ACS Energy Lett. 5(11):3357–61
- Zhao Q, Liu L, Yin J, Zheng J, Zhang D, et al. 2020. Proton intercalation/de-intercalation dynamics in vanadium oxides for aqueous aluminum electrochemical cells. *Angew. Chem. Int. Ed.* 59(8):3048–52
- Wu D, Housel LM, Kim SJ, Sadique N, Quilty CD, et al. 2020. Quantitative temporally and spatially resolved X-ray fluorescence microprobe characterization of the manganese dissolution-deposition mechanism in aqueous Zn/α-MnO₂ batteries. *Energy Environ. Sci.* 13(11):4322–33
- Akbashev AR. 2022. Electrocatalysis on oxide surfaces: fundamental challenges and opportunities. Curr. Opin. Electrochem. 35(1):101095
- Burke MS, Enman LJ, Batchellor AS, Zou S, Boettcher SW. 2015. Oxygen evolution reaction electrocatalysis on transition metal oxides and (oxy)hydroxides: activity trends and design principles. *Chem. Mater.* 27:7549–58
- Trotochaud L, Boettcher SW. 2014. Precise oxygen evolution catalysts: status and opportunities. Scr. Mater. 74:25–32
- Nellist MR, Laskowski FAL, Lin F, Mills TJ, Boettcher SW. 2016. Semiconductor–electrocatalyst interfaces: theory, experiment, and applications in photoelectrochemical water splitting. Acc. Chem. Res. 49(4):733–40
- Mefford JT, Akbashev AR, Kang M, Bentley CL, Gent WE, et al. 2021. Correlative operando microscopy of oxygen evolution electrocatalysts. *Nature* 593:67–73
- 83. Kang Q, Vernisse L, Remsing RC, Thenuwara AC, Shumlas SL, et al. 2017. Effect of interlayer spacing on the activity of layered manganese oxide bilayer catalysts for the oxygen evolution reaction. *J. Am. Chem. Soc.* 139:1863–70
- 84. Thenuwara AC, Shumlas SL, Attanayake NH, Aulin YV, McKendry IG, et al. 2016. Intercalation of cobalt into the interlayer of birnessite improves oxygen evolution catalysis. ACS Catal. 6:7739–43
- Thenuwara AC, Cerkez EB, Shumlas SL, Attanayake NH, McKendry IG, et al. 2016. Oxygen evolution reaction nickel confined in the interlayer region of birnessite: an active electrocatalyst for water oxidation. *Angew. Chem. Int. Ed.* 55:10381–85
- Lucht KP, Mendoza-Cortes JL. 2015. Birnessite: a layered manganese oxide to capture sunlight for water-splitting catalysis. J. Phys. Chem. C. 119(40):22838–46
- Peng H, McKendry IG, Ding R, Thenuwara AC, Kang Q, et al. 2017. Redox properties of birnessite from a defect perspective. PNAS 114(36):9523–28
- Ding R, Yasini P, Peng H, Perdew JP, Borguet E, Zdilla MJ. 2021. Reimagining the eg¹ electronic state
 in oxygen evolution catalysis: oxidation-state-modulated superlattices as a new type of heterostructure
 for maximizing catalysis. Adv. Energy Mater. 11(41):2101636
- Bhullar RK, Zdilla MJ, Klein ML, Remsing RC. 2021. Effect of water frustration on water oxidation catalysis in the nanoconfined interlayers of layered manganese oxides birnessite and buserite. J. Mater. Chem. A. 9(11):6924–32

- Spencer MA, Fortunato J, Augustyn V. 2022. Electrochemical proton insertion modulates the hydrogen evolution reaction on tungsten oxides. 7. Chem. Phys. 156(6):064704
- Yang C, Rousse G, Svane KL, Pearce PE, Abakumov AM, et al. 2020. Cation insertion to break the activity/stability relationship for highly active oxygen evolution reaction catalyst. Nat. Commun. 11:1978
- 92. Srimuk P, Su X, Yoon J, Aurbach D, Presser V. 2020. Charge-transfer materials for electrochemical water desalination, ion separation and the recovery of elements. *Nat. Rev. Mater.* 5:517–38
- 93. Alkhadra MA, Su X, Suss ME, Tian H, Guyes EN, et al. 2022. Electrochemical methods for water purification, ion separations, and energy conversion. *Chem. Rev.* 122(16):13547–635
- Byles BW, Hayes-Oberst B, Pomerantseva E. 2018. Ion removal performance, structural/compositional dynamics, and electrochemical stability of layered manganese oxide electrodes in hybrid capacitive deionization. ACS Appl. Mater. Interfaces 10(18):32313–22
- 95. Byles BW, Cullen DA, More KL, Pomerantseva E. 2018. Tunnel structured manganese oxide nanowires as redox active electrodes for hybrid capacitive deionization. *Nano Energy* 44:476–88
- 96. Ghodbane O, Ataherian F, Wu N-L, Favier F. 2012. In situ crystallographic investigations of charge storage mechanisms in MnO₂-based electrochemical capacitors. *J. Power Sources* 206:454–62
- Ghodbane O, Pascal J-L, Favier F. 2009. Microstructural effects on charge-storage properties in MnO₂-based electrochemical supercapacitors. ACS Appl. Mater. Interfaces 1(5):1130–39
- 98. Jin J, Li M, Tang M, Li Y, Liu Y, et al. 2020. Phase- and crystallinity-tailorable MnO₂ as an electrode for highly efficient hybrid capacitive deionization (HCDI). ACS Sustain. Chem. Eng. 8(30):11424–34
- Lee J, Srimuk P, Aristizabal K, Kim C, Choudhury S, et al. 2017. Pseudocapacitive desalination of brackish water and seawater with vanadium-pentoxide-decorated multiwalled carbon nanotubes. ChemSusChem 10(18):3611–23
- Fortunato J, Peña J, Benkaddour S, Zhang H, Huang J, et al. 2020. Surveying manganese oxides as electrode materials for harnessing salinity gradient energy. Environ. Sci. Technol. 54(9):5746–54
- Johnson EA, Post JE. 2006. Water in the interlayer region of birnessite: importance in cation exchange and structural stability. Am. Miner. 91:609–18